Observation of dynamic annealing effects in oxide single crystals after high-dose $^{18}O^{+}$ implantation at 500 °C

Yupu Li,* R. J. Liu, and Wei-Kan Chu
Texas Center for Superconductivity and Department of Physics, University of Houston, Houston, Texas 77204-5932

T. J. Tate
Department of Electronic and Electrical Engineering, Imperial College of Science Technology and Medicine, London SW7 2BT, United Kingdom

(Received 3 July 1997; revised manuscript received 9 October 1997)

Dynamic annealing effects and the behavior of oxygen trapping and migration in the perovskite oxide single crystals following high dose $^{18}O^{+}$ implantation at 500 °C and at room temperature have been studied. We report that the cascade collision induced by room-temperature irradiation with ^{18}O ions (200 keV $5\times10^{16}/cm^{2}$) into $SrTiO_3$ single crystal induces an essentially amorphous ($\chi_{min}\approx96\%$) surface layer to a depth of 400 nm. However, irradiation at 500 °C results in dynamic annealing effects since ion channeling shows χ_{min} of 3% in the near surface region. ^{18}O depth profiles measured by the $^{18}O(p,\alpha)^{15}N$ nuclear reaction show that high-temperature implantation results in a flat-topped ^{18}O distribution with only 48% (compared with room-temperature implantation) of implanted ^{18}O retained, and more importantly, channeled nuclear reaction analysis shows that at least 77% of the retained ^{18}O occupies substitutional sites. Room-temperature implantation plus post-irradiation annealing at 500 °C in flowing oxygen ambient resulted in much less recovery of irradiation damage ($\chi_{min}\approx33$ to 72%). Similar effects were observed in ^{18}O implanted single crystal $LaAlO_3$. [S0163-1829(98)03510-3]

I. INTRODUCTION

A wide range of materials can be modified advantageously by ion beams. During implantation, target temperature is a critical parameter. In the field of ion implantation into Si, in the literature it has been reported that high-temperature implantation can result in dynamic recovery of irradiation damage and redistribution of implanted atoms. For example, high dose O^{+} implantation into Si wafers (500–700 °C) followed by high-temperature annealing (1300–1405 °C) has been used to produce Si film on buried SiO_2 substrates for advanced complementary metal-oxide semiconductor circuits.[1–6] Room-temperature implantation results in such a high level of irradiation damage in the top silicon layer that high quality silicon thin films cannot be made, even by high-temperature annealing.[1–6] This demonstrates the necessity for, and advantage of implantation at a high target temperature. In a previous publication,[7] we reported some advantages and indirect evidence regarding dynamic annealing effects during high-temperature implantation of Ag^{+} into $YBa_2Cu_3O_{7-\delta}$ (YBCO) oxide films. In this case, oxygen starts migrating at a (lower) temperature between 250 and 300 °C.[8] The oxygen displacements from chain sites will result in loss of superconductivity and increase of oxygen vacancies in the film, which lead to structural defects. For this reason, it was necessary to perform *in situ* oxygen annealing to attain oxygen enrichment and ordering in YBCO films.[7] These facts prevent direct observation of dynamic annealing effects. The perovskite oxides $SrTiO_3$ and $LaAlO_3$ are useful substrates for epitaxial growth of high quality YBCO films. Each contains three elements and has perovskite structure (however belonging to the cubic system), and so provides ideal samples for the study of dynamic annealing effects in oxide single crystals. Ion implantation can be used to produce an ion-beam damaged surface for subsequent epitaxial growth of YBCO films. In this case, the damaged layer may exhibit some selected defects that are useful for studying the microwave loss mechanisms. This interest of ion implantation has been heightened by the observation of colossal magnetoresistance in the perovskite oxides,[9] which offers the possibility of developing a new generation of thin-film recording heads. Despite a substantial corpus of work on ion implantation of oxides, including high T_c oxide materials[10] and oxygen ionic conducting oxides,[11,12] the advantages and dynamic annealing effects of *high-temperature implantation* into the perovskite oxides have not yet been investigated and exploited. We note a recent publication[12] reporting that high-temperature implantation causes radiation-enhanced annealing as well as radiation-enhanced diffusion of implanted La into TiO_2 (i.e., rutile, which is a hard and chemically resistant coating material). In that case, the high-temperature (827 °C) implantation resulted in almost complete recovery of the lattice disorder.[12]

II. EXPERIMENTAL

The materials investigated in this work were one-side polished commercial (100) $SrTiO_3$ and $LaAlO_3$ single crystals. The stable oxygen isotope ^{18}O was implanted at 200 keV to a dose of 5×10^{16} ions/cm^2, at 7° to the surface normal to minimize channeling effects, *at* (1) *room-temperature* (RT) *and* (2) 500 °C. The beam current density was about 1×10^{-4} A/cm^2 (equivalent to 6.25×10^{14} ions/cm^2 s), and the 8 cm^2 target was in the beam for a total of 12 min. Because

0163-1829/98/57(10)/5668(6)/$15.00 © 1998 The American Physical Society

of the design of the target scanning system, in which the target is moved through a stationary beam, the use of beam time is very inefficient, and the total implantation time was about 1 h. RT and elevated-temperature samples were mounted side-by-side in order to achieve identical concurrent implantation conditions. Post-irradiation annealing was performed, at 500 °C for 45 min, in flowing natural oxygen ambient. The crystallinity of as-implanted and annealed materials was investigated by Rutherford backscattering spectrometry (RBS) and ion channeling analysis, using a 10 nA beam of 2.0 MeV $^4He^+$ at a scattering angle of 165°. Ag paste was painted onto the sample edge, and no surface charging effects were observed under the beam. ^{18}O depth profiles were measured using the $^{18}O(p,\alpha)^{15}N$ nuclear reaction analysis (NRA) (Refs. 13 and 14) at a proton energy of 730 keV. The Q of this convenient reaction was such that the energy of the α particles emitted is 3.394 MeV. A scattering angle of 150° was used, with the sample tilted at 35° to the beam in order to improve depth resolution. A standard Rutherford backscattering setup was used for the analysis. In our case, the depth resolution is about 17 nm at the surface and about 24 nm at the depth of 500 nm. Energy calibration was performed through RBS analysis of the oxide samples. Some channeled NRAs were also performed at a scattering angle of 150° with zero sample tilt in order to estimate the percentage of ^{18}O retained in substitution sites.

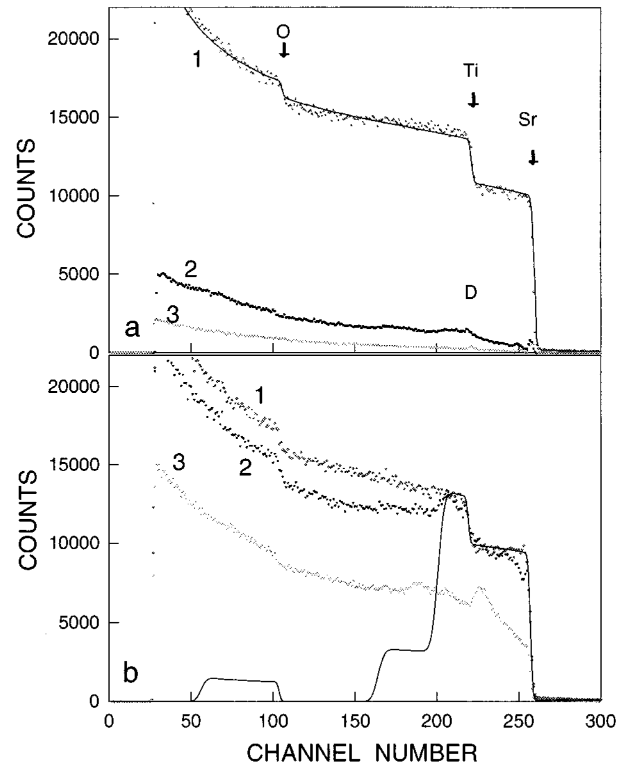

FIG. 1. (a) Lines 1 and 2: random and channeled RBS spectra (2.0 MeV $^4He^+$, $\theta = 165°$) for 500 °C implanted $SrTiO_3$. Line 3: channeled RBS spectrum for unimplanted $SrTiO_3$. Solid line: simulated random RBS spectrum. (b) Lines 1 and 2: random and channeled RBS spectra for (RT) implanted $SrTiO_3$. Line 3: channeled RBS spectrum for RT implanted $SrTiO_3$ after post-irradiation annealing. The solid line: simulated random RBS spectrum for 400 nm-thick $SrTiO_3$ plotted with arbitrary vertical units. This spectrum provides a reference to determine the depth of the damage. The energy calibration for these measurements: Energy (keV) $= 6.13 \times$ Channel number $+ 81.03$.

III. RESULTS AND DISCUSSION

Random (line 1) and channeled (line 2) RBS spectra are presented for 500 °C [Fig. 1(a)], and RT [Fig. 1(c)] $^{18}O^+$ implanted $SrTiO_3$, together with the channeled spectra for the initial unirradiated sample ($\chi_{min} \approx 0.8\%$ in the surface region) [line 3, Fig. 1(a)] and the post-irradiation annealed RT sample [line 3, Fig. 1(b)]. The solid lines in Fig. 1 show the random spectra for bulk $SrTiO_3$ [Fig. 1(a)] and 400 nm $SrTiO_3$ [Fig. 1(b)] simulated by RBX code,[15] plotted with arbitrary vertical units to provide a depth reference for the damage.

Figure 2 shows the α particle energy spectrum from the RT implanted sample. In the inset, the calibrated depth profiles are shown for the RT (line 1) and 500 °C (line 2) samples, obtained under identical NRA conditions. The conversion from energy spectrum, i.e., count vs energy of emitted α particles) to depth profile (i.e., relative count vs depth) is achieved by using the stopping power of α particles in $SrTiO_3$ calculated by TRIM-95 code,[16] while the effect of the change in the nuclear reaction cross section on the count per channel, due to the energy loss of the protons in the implanted layer (~ 50 keV), was calibrated using a relative cross-section factor inferred from the reported cross section.[13]

The as-implanted ^{18}O and damage distributions for the RT sample are presented in Fig. 3. The NRA concentration (line 1) calibration assumes that after implantation the density of $SrTiO_3$ is unchanged and all the implanted ^{18}O (the nominal dose) has been trapped in the implanted region. The distribution is essentially skew-Gaussian and the ^{18}O concentration peak is at a depth of about 284 nm. Lines 2, 3, and 4 show simulated ^{18}O, vacancy, and dpa (displacements per atom) depth profiles.[16] The experimental and calculated

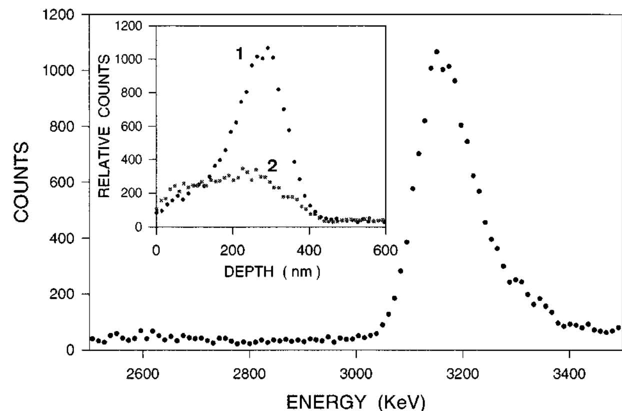

FIG. 2. Energy spectrum of α particles emitted from the $^{18}O(p,\alpha)^{15}N$ nuclear reaction with ^{18}O in RT implanted $SrTiO_3$. Inset: calibrated depth profiles (line 1 RT, line 2 500 °C). Measurements obtained with 35° sample tilt for improved depth resolution.

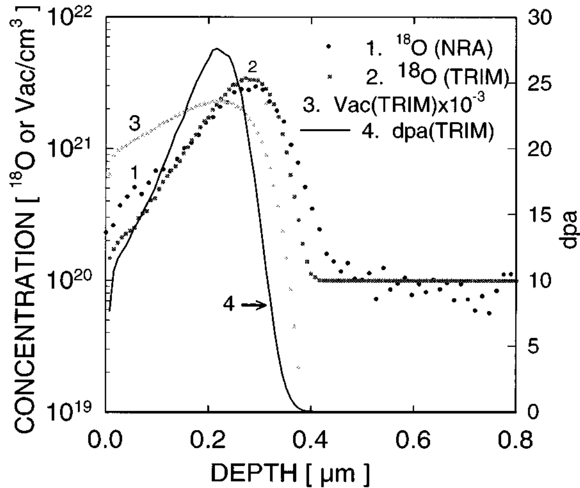

FIG. 3. Calibrated ^{18}O concentration distribution in RT implanted single crystal, measured by $^{18}O(p,\alpha)^{15}N$ nuclear reaction (line 1), compared with simulated ^{18}O concentration (line 2), vacancy (line 3), and dpa (line 4) distributions. The vacancy density has been multiplied by a factor of 10^{-3} to fit the same vertical scale. For calculating the damage distribution, a threshold displacement energy E_d of 20 eV has been assumed for all elements.

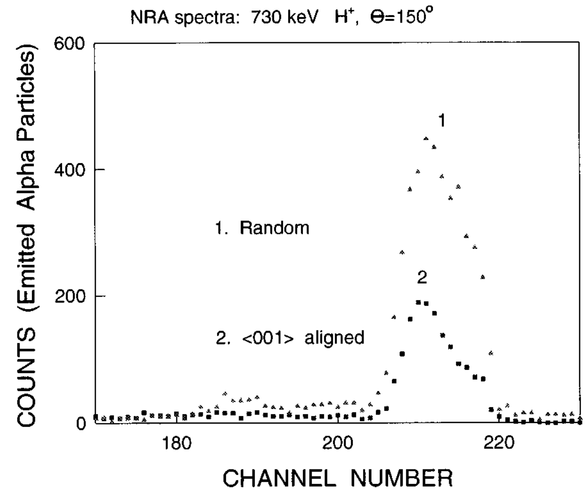

FIG. 4. Energy spectra of α particles emitted from the $^{18}O(p,\alpha)^{15}N$ nuclear reaction with ^{18}O in 500 °C implanted $SrTiO_3$, obtained with zero sample tilt angle. Line 1: the incident proton beam was not aligned; Line 2: the incident proton beam was aligned in the direction of ⟨001⟩ axis of the sample.

range data are in good agreement (see Table I), although the experimental profile is slightly wider than the simulated profile (see lines 1 and 2 in Fig. 3). The simulation predicts that near the damage peak, each target atom will on average have been displaced 28 times, and so it is to be expected that room-temperature implantation will amorphize the material. Indeed, lines 1 and 2 in Fig. 1(b) show that RT implantation results in an essentially amorphous layer to a depth of ~400 nm, $\chi_{\min}$ rapidly increasing from 81% at the surface to 96%. The depth of the damage layer is in very good agreement with the simulated dpa profile (see line 4 in Fig. 3).

In the case of 500 °C implantation, dynamic annealing effects are clearly visible, since $\chi_{\min}$ in the surface region is equal to 3% [Fig. 1(a)]. Here, we define dynamic annealing in a similar manner to Williams for high-temperature ion implanted Si.[17] During higher temperature implantations when defects (such as Frenkel pairs) produced by irradiation are mobile, defect annihilation and agglomeration occur synchronously with their production. At this stage, defect production competes with dynamic defect annealing in determining the resultant disorder structure. If the implantation temperature exceeds some threshold value, amorphization of the target materials is unlikely to occur since defect annealing dominates defect production. More importantly, high implantation temperatures may induce thermal redistribution of implanted species, in addition to the irradiation enhanced diffusion. Dynamic annealing effects are taken to include dynamic defect annealing and dynamic redistribution of implanted species during irradiation. In addition, clearly the definition of dynamic annealing is not only suitable to the implanted species of inert gas. The inset in Fig. 2 shows that the 500 °C implantation resulted in a flat-topped distribution accompanied by *in situ* release of ^{18}O. No indiffusion of ^{18}O into the undamaged region (i.e., beyond a depth of 500 nm) is observed (line 2, Fig. 2 inset). The total retained dose for the 500 °C implanted sample is about 48% of that for the RT implanted sample and so about 52% of implanted ^{18}O has been released from the sample *in situ*.

TABLE I. Range data including tabulated values of R_p (the depth of maximum ^{18}O concentration), $\bar{R}_p$ (the mean projected range), and ΔR_p^* (the "straggle"). The maximum ^{18}O concentration ($C_{\max}$) is also tabulated. R_d represents the depth of maximum vacancy concentration. It should be noted that here we define ΔR_p^* as the half width of the depth profile at the Au concentration $C = C_{\max}/e$. The density of $SrTiO_3$ has been chosen to be 5.12 g/cm^3.

200 keV $^{18}O^+$ 5×10^{16}/cm^2	R_p (nm)	R_d (nm)	$\bar{R}_p$ (nm)	ΔR_p^* (nm)	$C_{\max}$ (cm^{-3})
NRA Expt. ($SrTiO_3$)	284		255	106	2.8×10^{21}
TRIM-96 ($SrTiO_3$)	272	216	248	88	3.4×10^{21}

Lines 1 and 2 in Fig. 4 show random and channeled NRA spectra from the 500 °C implanted sample. The depth resolution is not as high as in Fig. 2 since the sample was not tilted during analysis. The ratio of areas under lines 2 and 1 between channels 200 and 224 in Fig. 4 (i.e., measurements of emitted α particles from the implanted layer under channeled and random conditions) is equal to 36% (i.e., χ_{impurity} measured by the NRA). However, this does not mean that only 64% of the retained ^{18}O are in substitutional sites, since the dechanneling effect on low-energy (730 keV) protons is much clearer than that for 2.0 MeV $^4He^+$ as shown in lines 1 and 2 in Fig. 5 (RBS spectra for the 500 °C implanted sample). In the implanted layer, $\chi_{\min}$ measured with a proton beam increases from 10 to 24% (i.e., the averaged χ_{host} measured by the RBS is equal to 17%), while the 2.0 MeV $^4He^+$ beam yield increases from 3 to 10% (lines 1 and 2 in Fig. 1). In addition, $\gamma_{\min}$ (2.0 MeV $^4He^+$) measured in the same region of the unirradiated perfect crystal also increases from about 1 to 4%. That means that the dechanneling effect of the proton beam has made a significant contribution to the

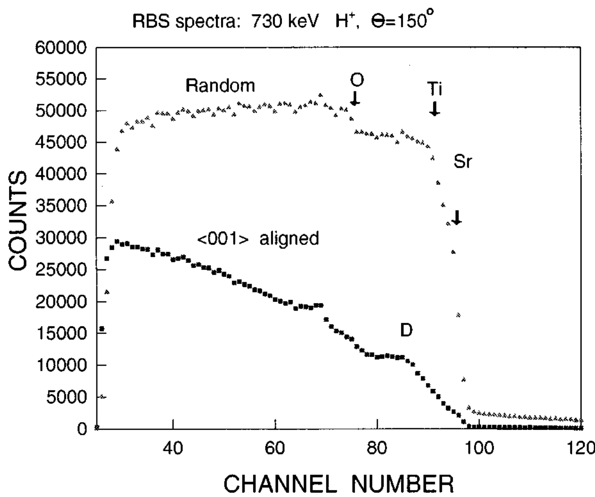

FIG. 5. Random and channeled RBS spectra (730 keV H^+, $\theta=150°$) for 500 °C implanted $SrTiO_2$. The energy calibration for the measurements: Energy (keV) $=6.12\times$Channel number $+117.56$.

count obtained from the emitted α particle yield shown in line 2 in Fig. 4. Taking into account the correction due to the larger low-energy proton beam dechanneling, and χ_{min} for the initial perfect crystal, the percentage of ^{18}O retained in substitutional sites is 77%. We note that the application of the formula for substitutional lattice site occupation: $f=(1-\chi_{impurity})/(1-\chi_{host})$ can facilitate the above discussion and gives the same value of 77%. In addition, the actual percentage may be still larger since there may be further effects to consider for the channeled NRA spectrum. For example, single crystal Y-stabilized ZrO_2 (YSZ) annealed in an ^{18}O gas ambient, should retain all exchanged ^{18}O in substitutional sites, but is observed that channeled NRA yields a similar substitutional percentage in the YSZ sample to that in the 500 °C implanted $SrTiO_3$.[14] Therefore, we conclude that at least 77% of the retained ^{18}O atoms are in substitutional sites in the case of 500 °C implanted $SrTiO_3$. During 500 °C implantation, many point defects are generated that are annihilated by dynamic recovery processes, while some point defects remain to form extended defects. In particular, line 2 in Fig. 1(a) shows some residual damage in the region around mark D. It seems that much of the retained ^{18}O has exchanged sites with ^{16}O in the 500 °C implanted sample, since the material remains as good quality single crystal. In this case, the extra oxygen (^{18}O and ^{16}O, i.e., the number excess above stoichiometric $SrTiO_3$) has escaped from the sample, probably forming gaseous oxygen molecules. For the RT implanted sample, which is essentially amorphous, the extra oxygen is retained, since there is little thermal energy for activating its diffusion and release. In fact, $SrTiO_3$ (density 5.12 g/cm^3), contains 5.1×10^{22} O/cm^3 and so a layer 19.7 nm thick will contain 1×10^{17} oxygen atoms/cm^2. The natural abundances are 99.76% ^{16}O and 0.2% ^{18}O, and so the implanted dose (5×10^{16} $^{18}O^+$/cm^2) only corresponds to 2% of the total oxygen already present in the implanted region of $SrTiO_3$ ($\sim$500 nm).

We report here on self-implantation of oxygen, a species already present in the target. After RT implantation, the implanted region is essentially amorphous. It seems that no oxygen outdiffusion occurred in these cases[18,19] although the damage within the implanted region is attributable to oxygen displacement. The 500 °C implantation resulted in a rather different case: the simulated damage of 28 dpa is no longer meaningful because of dynamic annealing effects. Either the threshold damage level for amorphization was not reached or else the energy deposition threshold for amorphization increases[17] as a result of dynamic annealing. It should be noted that during high-temperature implantation some of the energy deposition of the implanted ions resulted in defect annihilation and agglomeration whereas it results mainly in defect production for RT implantation. As we have mentioned that only 48% implanted ^{18}O remained in the sample and at least 77% of this retained ^{18}O occupied substitutional sites. The material remained as good quality single crystal and the cubic structure of $SrTiO_3$ is stable, thus, it can be expected that most of the replaced ^{16}O (i.e., those ^{16}O atoms with their lattice sites having been taken by the implanted ^{18}O atoms through oxygen isotopic exchange) will diffuse out of the sample. In other words, the total released ^{16}O is about 1.8×10^{16}/cm^2 and total released ^{18}O is about 2.6×10^{16}/cm^2 (i.e., 52% of the implanted dose). We assume that about 23% of the replaced ^{16}O could be trapped by residual defects rather than being released (on the basis that about 23% of the retained ^{18}O occupied non-substitutional sites), and so the total released ^{16}O amounts to about 1.4×10^{16}/cm^2 (or 0.56% of the total oxygen already in the implanted layer). However, it should be noted that we have no analytic technique to monitor such relative change of the absolute ^{16}O content. We can monitor $\geqslant2\%$ of relative change of the absolute ^{16}O content in the surface region of the implanted layer by 3.05 MeV $^4He^+$ RBS.

Naguib and Kelly[20,21] have investigated implantation of nonmetallic solids and proposed a formalism using a modified thermal spike model, to predict whether the final material will be amorphous or crystalline. Atoms in the cascade volume are in a transient, pseudo-liquid state surrounded by the original lattice. As the perturbation relaxes, the crystallization front propagates a distance x_c inwards from the surrounding lattice. If x_c is greater than the mean atomic spacing λ, then the materials will crystallize. x_c has an explicit dependence on the bulk temperature, T_∞:

$$x_c \propto (1-T_\infty/T_m)^{-8/3},$$

where T_m is the melting temperature. Putting in values for $SrTiO_3$ $T_m=2353$ K, $T_\infty(\mathrm{low})=300$ K and $T_\infty(\mathrm{high})=773$ K, the model predicts an increase in x_c of a factor of 2.0 at the high-temperature implantation. If we apply this model to our case, we may conclude that during 500 °C implantation x_c is greater than λ and so most of the irradiation damage is annihilated as it forms and good crystalline order is maintained after implantation.

C. W. White *et al.*[22] report good regrowth at a rather low temperature of $SrTiO_3$ amorphized by Pb^+ implantation (540 keV, 1×10^{15}/cm^2 at 125 K). This implantation resulted in disorder in both metal cation sublattices to produce the amorphous state, corroborating our findings for RT $^{18}O^+$ implanted $SrTiO_3$ [see lines 1 and 2 in Fig. 1(b)]. In fact, the oxygen sublattice has also been damaged but it cannot be

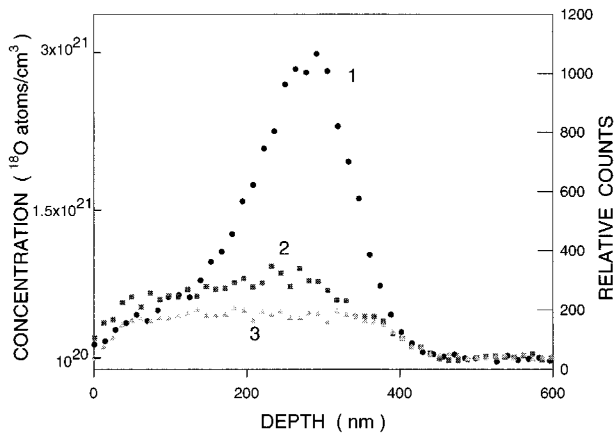

FIG. 6. Calibrated ^{18}O concentration distribution profile for implanted $SrTiO_3$: RT (line 1), 500 °C (line 2), RT implant and post-anneal (line 3).

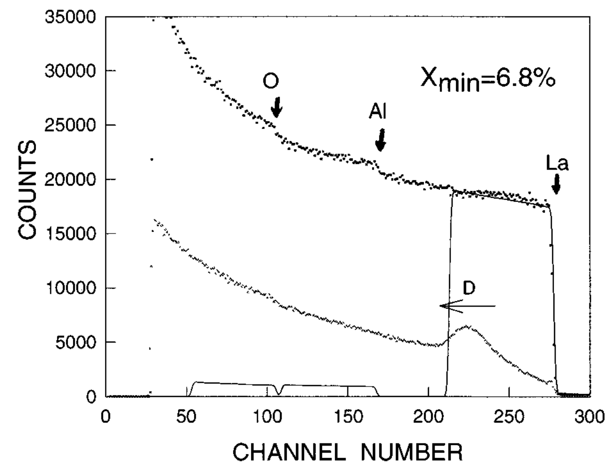

FIG. 7. Lines 1 and 2: random and channeled RBS spectra (2.0 MeV $^4He^+$, $\theta = 165°$) from 500 °C implanted $LaAlO_3$ oxide single crystal. The solid line: simulated random RBS spectrum for 400 nm-thick $LaAlO_3$, plotted with arbitrary vertical units. This spectrum provides a reference to determine the depth of the damage. The energy calibration for these measurements: Energy (keV) = 6.13 × Channel number + 81.03.

observed by RBS. Therefore, during the lower temperature implantation, the displacement of target atoms resulted in amorphization since defect production dominated the process. The amorphous layer induced by ion implantation in oxides recrystallizes epitaxially by furnace heating, the activated process proceeding from an underlying seed crystal. With the assumption that the observed epitaxial recrystallization of annealed Pb^+ implanted sample (in air) is a thermally activated process White *et al.*[22] obtained a rather low activation energy of 0.77 eV. It can be expected from the regrowth curve reported by them[22] that epitaxial regrowth could proceed at a temperature as low as 225 °C. It is also interesting to compare this with our result obtained from 500 °C $^{18}O^+$ implanted $SrTiO_3$. Our implantation temperature is much higher than the critical regrowth temperature during the post-irradiation annealing. Moreover, during high-temperature irradiation the annihilation and agglomeration of point defects are more probable than during post-irradiation annealing: the effect of dynamic annealing is that the sample was never amorphized. RBS and ion channeling studies [Fig. 1(a)] showed that some extended defects (such as dislocation loops) remained within the implanted layer especially near the end of the range. However, the defect density is much lower than in the post-irradiation annealed sample (i.e., annealed at similar temperature, see below). In addition, even following higher temperature post-irradiation annealing, the regrown amorphous layer may be more granular than the initial layer[23] or the layer formed by the high-temperature implantation. Positive confirmation of the detailed defect structures will require cross sectional transmission electron microscopy observations.

Calibrated ^{18}O concentration distributions are shown in Fig. 6 for 500 °C (line 2), RT (line 1), and RT plus 500 °C annealed (line 3) samples. Note that the ^{18}O dose retained after post-irradiation annealing (Fig. 6, line 3) is only 34% for that in the RT sample (Fig. 6, line 1). It can be seen [Fig. 1(b), line 3] that χ_{min} is equal to 33% at the top surface increasing to 72% at a depth of 230 nm. It is clear that the RT implantation and post-irradiation annealing resulted in much less recovery of damage, in spite of the NRA (line 3 in Fig. 6) observation showing diffusion and exchange of about 66% of the retained ^{18}O with ^{16}O in the annealing ambient. The quantity of ^{18}O released is greater than that for the 500 °C implanted sample. Following RT implantation most of the retained ^{18}O atoms are weakly and become more unstable during post-irradiation annealing. In addition, the hump around the mark *d* (at a depth of ~465 nm) in Fig. 1(b) shows some residual end-of-range defects formed at the interface region between the implanted and unimplanted layers. These results illustrate that dynamic annealing effects are very different from post-irradiation annealing effects, since amorphized material requires thermal energy to contribute both to (1) recovery of crystallinity and (2) activation of the implanted species. For better recovery of the damage, a higher post-irradiation annealing temperature must be chosen. Even so, when the amorphized layer recrystallizes, it normally contains disoriented regions and thus is more granular than the initial single crystal, leading to a deterioration in material quality. The dynamic annealing in the crystalline material implanted at high temperature may be seen as an increase in the effective threshold energy density for amorphization[17] since defect annealing dominates defect production. Some extended defects may remain in the material as a result of agglomeration of point defects. Note that in our case the total implantation processing time was about 1 h, allowing plenty of time for dynamic annealing.

It would be of interest also to compare our post-irradiation annealing data with the results of C. W. White *et al.*[22] For the Pb^+ implanted $SrTiO_3$ sample (540 keV, $1 \times 10^{15}/cm^2$ at 125 K) White *et al.* reported that the annealing condition (400 °C 30/min, in air) is sufficient to achieve complete epitaxial crystallization of the amorphous layer. The value of χ_{min} behind the surface peak is about 9% in their Fig. 45, which is better than 33% for our RT implanted $SrTiO_3$ after post-irradiation annealing [500 °C/45 min, in flowing oxygen ambient Fig. 1(b), line 3]. It seems that White *et al.* achieved better recovery at a lower annealing

temperature, probably due to the different ''amorphous'' defect structures obtained by heavy (Pb^+) and light (O^+) ion irradiation. White *et al.* noted that although the damage layer crystallized epitaxially, the regrown layer has a high density of defects relative to the unimplanted near-surface region because the aligned RBS count in the implanted region after annealing is considerably greater than that in the unimplanted region.[22]

In addition, our research shows similar dynamic annealing for ^{18}O implanted $LaAlO_3$ at 500 °C. Figures 7(a) and 7(b) shows random and channeled RBS spectra from 500 °C implanted $LaAlO_3$ (200 keV $^{18}O^+$, $5\times10^{16}/cm^2$). Identical RT irradiation produced an essentially amorphous layer to a depth of $\sim$400 nm.[24] Dynamic recovery of the damage is slightly less effective than in $SrTiO_3$, as χ_{min} is about 6.8% for the $LaAlO_3$ and about 3% for $SrTiO_3$, and also the residual damage region (see the region marked with *D* in Fig. 5) is more pronounced in $LaAlO_3$. Single crystal $LaAlO_3$ is highly twinned and the $SrTiO_3$ is not, which could be an explanation of the above observation.

IV. SUMMARY

Single crystal $SrTiO_3$ has been irradiated with 200 keV ^{18}O ions to a dose of $5\times10^{16}/cm^2$, at room temperature and 500 °C. Implantation at 500 °C resulted in dynamic annealing effects, ion channeling showing χ_{min} of 3% in the near-surface region. An important observation is that the retained ^{18}O in the sample shows a flat-topped distribution and at least 77% of the retained ^{18}O occupies substitutional sites. Similar effects are observed in single crystal $LaAlO_3$. We conclude that suitable high-temperature implantation can be applied to (1) dope impurities into oxide single crystals without amorphization and (2) control the residual damage level and redistribution of implanted ions.

ACKNOWLEDGMENTS

This work was supported by ARPA MDA 972-90-J-1001 and the State of Texas through the Texas Center for Superconductivity at the University of Houston. This research was also supported in part by the MRSEC program of the National Science Foundation under Award No. DMR-9632667.

*Present address: Charles Evans and Associates, 301 Chesapeake Drive, Redwood City, CA 94063.

[1] K. Izumi, M. Doken, and H. Ariyoshi, Electron. Lett. **14**, 593 (1978).
[2] P. L. F. Hemment, in *Semiconductor-on-Insulator and Thin Film Transistor Technology*, edited by A. Chiang, N. W. Geis, and L. Pfeiffer (Materials Research Society, Pittsburgh, 1986), p. 207.
[3] G. K. Celler, Proc. Electrochem. Soc. **90-7**, 472 (1990).
[4] M. A. Gurra, Proc. Electrochem. Soc. **90-6**, 21 (1990).
[5] S. Nakashima and K. Izumi, J. Mater. Res. **8**, 523 (1993).
[6] Yupu Li, J. A. Kilner, A. Nejim, P. L. H. Hemment, and C. D. Marsh, Nucl. Instrum. Methods Phys. Res. B **99**, 479 (1995).
[7] Yupu Li, J. R. Liu, X. T. Cui, J. Z. Qu, Q. Chen, and Wei-Kan Chu, Appl. Phys. Lett. **70**, 3029 (1997).
[8] Yupu Li, J. A. Kilner, T. J. Tate, M. J. Lee, R. J. Chater, H. Fox, R. A. De Souza, and P. G. Quincey, Phys. Rev. B **51**, 8498 (1995).
[9] S. Jin, T. H. Tiefel, M. McCormack, R. A. Gastnacht, R. Ramesh, and L. H. Chen, Science **264**, 413 (1994).
[10] L. E. Rehn, Nucl. Instrum. Methods Phys. Res. B **64**, 161 (1992).
[11] A. J. Burggraaf, P. J. Gellings, and D. Scholten, in *High Tech. Ceramics*, edited by P. Vincenzini (Elsevier, Amsterdam, 1987), pp. 779–794.
[12] B. A. van Hassel and A. J. Burggraaf, Appl. Phys. A: Solids Surf. **49**, 33 (1989).
[13] G. Amsel, J. P. Nadai, E. D'Artemaire, D. David, E. Girard, and J. Moulin, Nucl. Instrum. Methods **92**, 481 (1971).
[14] J. R. Liu, Yupu Li, Q. Chen, X. T. Cui, R. Christofferson, A. Jacobson, and W. K. Chu, Nucl. Instrum. Methods (to be published).
[15] E. Kctai, *RBX code* (Sky-Soft Ltd., Budapest, 1995).
[16] J. F. Ziegler, J. P. Biersack, and U. Littmark, *The Stopping and Ranges of Ions in Solids* (Pergamon, New York, 1985).
[17] J. Williams, MRS Bull. **6**, 47 (1992), and references therein.
[18] G. J. Clark, A. D. Marwick, R. H. Hoch, and R. B. Laibowitz, Appl. Phys. Lett. **51**, 139 (1987).
[19] O. Meyer, T. Kroener, J. Remmel, J. Geerk, G. Linker, B. Strehlau, and Th. Wolf, Nucl. Instrum. Methods Phys. Res. B **65**, 539 (1992).
[20] H. M. Naguib and R. Kelly, Radiat. Eff. **25**, 1 (1975).
[21] R. Kelly, in *Ion Bombardment Modification of Surfaces*, edited by O. Auciello and R. Kelly (Elsevier, New York, 1984), pp. 79–126.
[22] C. W. White, C. J. McHargue, P. S. Sklad, L. A. Boatner, and G. C. Farlow, Mater. Sci. Rep. **4**, 99 (1989); see also, C. W. White, L. A. Boatner, J. Rankin, and M. J. Aziz, in *Materials Modification and Growth Using Ion Beams*, edited by V. Gibson, A. E. White, and P. P. Pronko, MRS Symposia Proceedings No. 93 (Materials Research Society, Pittsburgh, 1987), p. 11.
[23] T. J. Tate, M. J. Lee, Yupu Li, J. A. Kilner, Y. H. Li, C. A. Leach, D. Lacey, A. D. Caplin, R. E. Somekh, P. Przyslupski, and P. G. Quincey, Physica C **235-240**, 569 (1994).
[24] Yupu Li, J. A. Kilner, T. J. Tate, R. J. Chater, C. Jeynes, and Z. H. Jafri, Nucl. Instrum. Methods Phys. Res. B **118**, 133 (1996).